

Article

# Coordinated Symmetrical Altitude Position and Attitude Control for Stratospheric Airship Subject to Strong Aerodynamic Uncertainties

Kun Yan <sup>1</sup>, Ju Jiang <sup>1</sup>, Mingwei Sun <sup>2,\*</sup> and Zengqiang Chen <sup>2</sup> 

<sup>1</sup> College of Automation Engineering, Nanjing University of Aeronautics and Astronautics, Nanjing 211106, China; yankun@buaa.edu.cn (K.Y.); jiangju@nuaa.edu.cn (J.J.)

<sup>2</sup> College of Artificial Intelligence, Nankai University, Tianjin 300350, China; chenzq@nankai.edu.cn

\* Correspondence: sunmw@nankai.edu.cn

**Abstract:** The stratospheric airship has important value in both commercial and military use. The altitude position control is very crucial for the airship to conduct specific missions, which is also a challenge because of both the severe relative aerodynamic mismatches and the large lag due to the quite low speed of the airship within 15 m/s. In this paper, a coordinated altitude and attitude control method was proposed to realize satisfactory altitude position control while maintaining the attitude stability by properly employing the two actuators, the propeller thrust and the elevator, in a consistent manner. In this process, the references for the vertical speed and the pitch were specified in a straightforward way of proportionating them by considering their physical characteristics and the inherent symmetrical relationship between them, which can be obtained through the kinematics. An extended disturbance observer was used to eliminate the severe aerodynamic uncertainties to symmetrically distribute the two actuator outputs by dynamically decoupling the vertical speed and the pitch angular rate loops into the two independent integrators. As a result, the explicit proportional controllers were sufficient to realize efficient command tracking. Rigorous theoretical investigation was provided to symmetrically prove the quantitative bounded property of the estimation and tracking errors. The simulation results demonstrated the effectiveness of the proposed approach, which can realize a 500-m altitude difference tracking within 200 s with less than 0.5 deg/s pitch angular rate.

**Keywords:** stratospheric airship; coordinated control; symmetry; aerodynamic uncertainties; extended state observer; robustness



**Citation:** Yan, K.; Jiang, J.; Sun, M.; Chen, Z. Coordinated Symmetrical Altitude Position and Attitude Control for Stratospheric Airship Subject to Strong Aerodynamic Uncertainties. *Symmetry* **2023**, *15*, 1260. <https://doi.org/10.3390/sym15061260>

Academic Editor: Alexander Zaslavski

Received: 7 May 2023

Revised: 11 June 2023

Accepted: 13 June 2023

Published: 14 June 2023



**Copyright:** © 2023 by the authors. Licensee MDPI, Basel, Switzerland. This article is an open access article distributed under the terms and conditions of the Creative Commons Attribution (CC BY) license (<https://creativecommons.org/licenses/by/4.0/>).

## 1. Introduction

The stratosphere is the altitude range between 10 km and 50 km above the ground, and wherein the atmosphere mainly flows at the horizontal direction. Within this altitude range, the air tends to be dry, resulting in steady movement and providing excellent visibility with low humidity [1]. Exploiting these favorable conditions, the stratospheric airship emerges as an extraordinary aerostatic vehicle capable of flying at extremely low speeds for extended durations. Its prolonged airborne missions encompass a diverse array of applications, including communication, environmental monitoring, emergency rescue operations, and military scouting [2]. One of the primary advantages of the stratospheric airship lies in its utilization of lighter-than-air gas, which imparts buoyancy and enables ascent without significant power or fuel consumption. In contrast to conventional aircraft, the stratospheric airship operates as a low-dynamic flight vehicle, characterized by slow speed and minimal noise emissions. This unique attribute allows the airship to maintain a steady hover around a fixed position for prolonged periods [3]. In recent years, there has been a burgeoning interest in the design and development of modern stratospheric airships, primarily due to their exceptional commercial and military potential. These

vehicles possess distinctive advantages that set them apart from other aerial platforms, making them an attractive choice for a wide range of applications. The capability to remain airborne for extended periods, coupled with their versatility and operational flexibility, has garnered significant attention and propelled advancements in their design [4–6].

The stratospheric airship control is a crucial part that can determine the mission to be successful or not, which is restricted by the dynamic model, control strategy, and actuator configuration. Because there are strong nonlinearities, aerodynamic uncertainties, and complicated model variables, the following difficulties are present for control design [7]:

- (1) The dynamic model of the stratospheric airship is intricate, incorporating unmodeled dynamics, parametric uncertainties, and external disturbances. These factors introduce complexities that need to be accounted for in control system design, as they can impact the stability and performance of the airship.
- (2) The airship's characteristics, such as its large volume-to-mass ratio and slow speed, result in notable time lags, leading to sluggish control response. This delay poses challenges in achieving precise and timely control actions, necessitating careful consideration of control strategies to overcome this inherent limitation.
- (3) The aerodynamic efficiency of the airship at low dynamic pressure and low speed is insufficient. To address this issue, it becomes necessary to incorporate other appropriate actuators into the control system. These additional actuators can enhance the maneuverability and responsiveness of the airship, compensating for the limitations posed by its aerodynamic characteristics.
- (4) The control design for a stratospheric airship must address the inherent coupling of multiple physical variables. The trajectory and attitude of the airship are intricately interconnected, requiring careful coordination to ensure stable and accurate control. Managing the coupling between these variables is crucial to achieve desired flight performance and maneuverability.

For the stratospheric airship, the altitude position control is a popularly used mode. During this phase, the airship hovers at around a specific altitude with acceptable error range for a long time. This task seems quite commonplace for the traditional flight vehicle since it is just a cruise phase that can be easily realized in the high-speed mode. However, the speed of the airship is rather low such that the aerodynamic efficiency is not sufficient enough to support a fast altitude tracking capability, which can lead to a remarkable lagging altitude response. Consequently, stratospheric airships often experience long settling times and excessive overshoot when attempting to adjust and stabilize their altitude. Achieving a reasonably fast and steady altitude control becomes a crucial objective in the design of the airship's control system. The control system must overcome the limitations imposed by the airship's low aerodynamic efficiency and ensure precise control over the altitude parameter. To address these challenges, innovative control strategies and algorithms need to be employed. This entails the development of control techniques specifically tailored to the unique characteristics of stratospheric airships, accounting for their low-speed flight dynamics and aerodynamic inefficiencies. By incorporating these advanced control methodologies, it becomes possible to enhance the airship's altitude control capabilities, reducing settling times and overshoot, and ensuring a stable and accurate altitude maintenance. The successful realization of reasonably fast and steady altitude control for stratospheric airships holds paramount importance. It not only enables precise mission execution but also ensures the airship's operational efficiency and safety. Consequently, researchers and engineers working on control system design for stratospheric airships strive to overcome the challenges associated with altitude control, continuously exploring novel control strategies, and optimizing the performance of the control system to achieve superior altitude control characteristics. In [8], the global nonlinear control development of an autonomous airship was presented. The preliminary reports for the three nonlinear control solutions under investigation were presented, which are dynamic inversion, back-stepping, and the sliding mode control. A complete airship mission, with vertical take-off, path tracking, hovering, and vertical landing was successfully simulated

using the back-stepping approach. The altitude control belongs to the motion control in the longitudinal plane. Kusagaya proposed an optimal control based on the nonlinear feedback decoupling technique and applied it to the longitudinal control of an airship [9], which is not dependent on nonlinear Riccati equation or adjoint vector, avoiding complex computation and enhancing the accuracy. Guo proposed an altitude position control method based on adaptive sliding mode control and fuzzy logic with the combined configuration of propeller thrust and aerodynamic force [10], and the simulation results exhibited its good robustness to aerodynamic uncertainties and external disturbances. In [10], the control scheme was decomposed into an altitude subsystem and a vertical speed subsystem, and then the fuzzy logic was employed to tune the controller. In the previous investigations, the references for the altitude position and the pitch were separately specified and they were not inherently correlated according to the symmetry of the airship. In [11], the auxiliary air bursas charge or deflation and elevator combination control was employed to adjust the airship altitude for suspension, and the control law was designed based on fuzzy self-tuning control. The Q-learning and cerebella model articulation controller (CMAC) were utilized to realize the airship altitude reinforcement learning control based on the Markov decision process [12]. It should be noted that all these mentioned control algorithms are complicated in form with many parameters to tune, which are difficult to implement in practice. In fact, a practical PID-type controller is preferred in practice for the airship altitude control due to its maturity. On the other hand, the typical setup of the stratospheric airship control involves two actuators, with a traditional cascade control loop structure comprising an inner attitude loop and an outer altitude loop. This configuration poses a significant challenge: how to effectively coordinate and synchronize the actions of both actuators? Coordinating the operation of these two actuators is crucial for achieving precise control over the airship's altitude and maintaining its stability during flight. Schmidt characterized an airship's surge dynamics, modeled the wind environments, and developed and evaluated the simple control and guidance algorithms [13]. It was shown that the vehicle is dynamically stable and sluggish, and that significant thrust and control power might be required to stationkeep in turbulence. Therefore, several reference specifications might lead to inconsistency and the attitude stability cannot be ensured. In addition, the controller employed in the control system must effectively address the presence of relatively large aerodynamic uncertainties encountered in the stratosphere, wherein a conventional PID controller is difficult to cope with. Due to the complex and dynamic nature of the stratospheric environment, the airship is subjected to various uncertainties and disturbances that can affect its performance. To mitigate the impact of these uncertainties, the use of a disturbance observer has emerged as a practical and unique technique. Implementing a disturbance observer allows for the estimation and compensation of multiple uncertainties, enhancing the robustness of the control system [14,15]. It is worth noting that while there have been numerous investigations focused on horizontal trajectory tracking for airships [16–23], research specifically targeting the altitude position control for stratospheric airships has been relatively scarce. This disparity in research emphasis underscores the need for further exploration and development in this particular area, as precise altitude control is vital for the successful operation and mission fulfillment of stratospheric airships. Addressing the challenges associated with the altitude position control will contribute to advancing the overall capabilities and effectiveness of stratospheric airship control systems. Therefore, a practical and efficient airship altitude control strategy must be found to realize the decoupling and disturbance rejection function in an explicit manner.

In this paper, we proposed a comprehensive control strategy for the stratospheric airship. At first, according to the characteristics of the airship altitude position control, the vertical speed and pitch angular rate were selected as the control variables to speed up the dynamic performance for the naturally sluggish airship. The references for these two controlled variables were generated in a straightforward manner from the position to the speed control transformation perspective. The inherent symmetrical relation between the vertical speed and the pitch was utilized to yield the pitch reference, which is the coordination

in the guidance regard. As a result, the two-input-two-output plant could be decoupled into two single-input-single-output plants, and two extended state observers [24,25] were used to attenuate the uncertain aerodynamic effects as well as realize dynamic decoupling. In the meantime, two actuators could realize a coordinated and symmetrical control. The theoretical investigation was presented to quantitatively ensure the bounded estimation and the tracking errors symmetrically. The mathematical simulations demonstrated the effectiveness of the proposed method.

The remaining parts of the paper are organized as follows. The mathematical model of the stratospheric airship and the problem formulation are provided in Section 2. In Section 3, the coordinated guidance references and controller design are presented for the altitude position control. The closed-loop stability analysis is conducted in Section 4. The simulation results are offered in Section 5. Section 6 concludes the paper.

The contributions of the paper can be summarized as:

- (1) The symmetrical dynamics of airship is fully used to coordinate the pitch and the vertical speed references in an explicit manner.
- (2) A dynamic decoupling controller based on a disturbance observer is provided by utilizing the state transformation.

## 2. Mathematical Model of the Stratospheric Airship and Problem Formulation

For the altitude position control, the longitudinal dynamics is considered for brevity. The pure longitudinal equations are as follows [26–28]:

$$\begin{cases} (m + m_{33})\dot{w} - mx_G\dot{q} - mz_Gq^2 = G \cos \theta - B \cos \theta + T_z \\ + Q\Xi^{\frac{2}{3}}(-C_X \sin \alpha - C_Z \cos \alpha) \\ (I_y + m_{55})\dot{q} - mx_G\dot{w} = -z_G G \sin \theta - x_G G \cos \theta + Q\Xi C_m - l_x T_z \\ \dot{\theta} = q \\ \dot{h} = w \cos \theta \end{cases} \quad (1)$$

where  $w$  is the vertical speed (m/s),  $q$  is the pitch angular rate (rad/s),  $\theta$  is the pitch (rad),  $h$  is the altitude (m),  $\alpha$  is the angle of attack (rad),  $m$  is the mass of the airship (kg),  $m_{33}$  and  $m_{55}$  are the added masses (kg),  $I_y$  is the pitch moment of inertia (kg·m<sup>2</sup>),  $\Xi$  is the airship volume (m<sup>3</sup>),  $u$  is the forward speed (m/s),  $(x_G, z_G)$  is the coordinate of center of gravity (COG) in the body coordinate framework (m),  $l_x$  is the propeller axial position (m),  $T_z$  is the axial propeller thrust (N),  $C_X$  is the drag coefficient,  $C_Z$  is the lift coefficient,  $C_m$  is the pitch moment coefficient,  $G$  is the gravity (N),  $B$  is the buoyancy (N),  $Q = \frac{1}{2}\rho V^2$  is the dynamic pressure (Pa or N/m<sup>2</sup>),  $\rho$  is the air density (kg/m<sup>3</sup>),  $V = \sqrt{u^2 + w^2}$  is the speed of the airship (m/s). Here,  $C_X$ ,  $C_Z$ , and  $C_m$  are dimensionless coefficients.

Equation (1) can be reformulated into a compact state space form as

$$M\dot{x} = f(x) + g(x)u \quad (2)$$

with the state vector  $x = [w \ q \ \theta \ h]^T$  and  $u = [T_z \ \delta_e]^T$ , where  $\delta_e$  is the elevator (rad), as well as

$$M = \begin{bmatrix} m + m_{33} & -mx_G & 0 & 0 \\ -mx_G & I_y + m_{55} & 0 & 0 \\ 0 & 0 & 1 & 0 \\ 0 & 0 & 0 & 1 \end{bmatrix} \quad (3)$$

$$f(x) = \begin{bmatrix} f_1(x) \\ f_2(x) \\ f_3(x) \\ f_4(x) \end{bmatrix} = \begin{bmatrix} mz_Gq^2 - Q\Xi^{\frac{2}{3}}[(C_{X0} + C_X^\alpha) \sin \alpha + (C_{Z0} + C_Z^\alpha) \cos \alpha] \\ -z_G G \sin \theta - x_G G \cos \theta + mz_Gqw + Q\Xi(C_{m0} + C_m^\alpha + C_m^q) \\ q \\ w \cos \theta \end{bmatrix} \quad (4)$$

$$g(x) = [g_1(x)g_2(x)] = \begin{bmatrix} 1 & -Q\nabla^{\frac{2}{3}}C_Z^{\delta_e} \cos \theta \\ -l_x & Q\nabla C_m^{\delta_e} \\ 0 & 0 \\ 0 & 0 \end{bmatrix} \quad (5)$$

where  $C_Z^{\delta_e}$  and  $C_m^{\delta_e}$  are the partial derivatives of the lift and the pitch moment with respect to  $\delta_e$ , respectively, or they are the corresponding elevator efficiency factors. The related aerodynamic coefficients are calculated as

$$\begin{cases} C_X = C_{X_0} + C_X^\alpha \alpha \\ C_Z = C_{Z_0} + C_Z^\alpha \alpha + C_Z^{\delta_e} \delta_e \\ C_m = C_{m_0} + C_m^\alpha \alpha + C_m^q q + C_m^{\delta_e} \delta_e \end{cases} \quad (6)$$

Note that all the angular variables in (6) are used in the unit of radian alike. The two actuators have different roles in the regulation: the propeller thrust can achieve fast but rough regulation due to its large amplitude, while the elevator can realize slow but refined regulation due to its low efficiency.

The problem is to manipulate  $h$  from an initial altitude to a target altitude while maintaining the attitude stable by using the two actuators harmoniously.

### 3. Coordinated Control and Reference Design

#### 3.1. Coordinated Control Design

##### 3.1.1. Model Transformation

According to (2), one has

$$\dot{x} = M^{-1}f(x) + M^{-1}g(x)u \quad (7)$$

Because

$$M^{-1} = \begin{bmatrix} \frac{I_y + m_{55}}{(m + m_{33})(I_y + m_{55}) - m^2 x_G^2} & \frac{m x_G}{(m + m_{33})(I_y + m_{55}) - m^2 x_G^2} & 0 & 0 \\ \frac{m x_G}{(m + m_{33})(I_y + m_{55}) - m^2 x_G^2} & \frac{m + m_{33}}{(m + m_{33})(I_y + m_{55}) - m^2 x_G^2} & 0 & 0 \\ 0 & 0 & 1 & 0 \\ 0 & 0 & 0 & 1 \end{bmatrix} \quad (8)$$

then

$$M^{-1}g(x) = \begin{bmatrix} I_y + m_{55} & m x_G & 0 & 0 \\ m x_G & m + m_{33} & 0 & 0 \\ 0 & 0 & 1 & 0 \\ 0 & 0 & 0 & 1 \end{bmatrix} \frac{\begin{bmatrix} 1 & -Q\nabla^{\frac{2}{3}}C_Z^{\delta_e} \cos \theta \\ -l_x & Q\nabla C_m^{\delta_e} \\ 0 & 0 \\ 0 & 0 \end{bmatrix}}{[(m + m_{33})(I_y + m_{55}) - m^2 x_G^2]^2} \quad (9)$$

$$= \frac{\begin{bmatrix} I_y + m_{55} - m x_G l_x & -(I_y + m_{55})Q\nabla^{\frac{2}{3}}C_Z^{\delta_e} \cos \theta + m x_G Q\nabla C_m^{\delta_e} \\ m x_G - (m + m_{33})l_x & -m x_G Q\nabla^{\frac{2}{3}}C_Z^{\delta_e} \cos \theta + (m + m_{33})Q\nabla C_m^{\delta_e} \\ 0 & 0 \\ 0 & 0 \end{bmatrix}}{[(m + m_{33})(I_y + m_{55}) - m^2 x_G^2]^2}$$

Since the last two rows of  $M^{-1}g(x)$  are completely null, we can reduce (7) into a second-order subsystem with two virtual inputs as

$$\dot{z} = h(x) + v \quad (10)$$

where  $z = [w \ q]^T$ ,  $h(x) = M^{-1}f(x) = [h_1(x) \ h_2(x)]^T$ , and

$$v = \begin{bmatrix} v_1 \\ v_2 \end{bmatrix} = \frac{\begin{bmatrix} (I_y + m_{55} - mx_G l_x) T_z + [mx_G Q \nabla C_m^{\delta_e} - (I_y + m_{55}) Q \nabla^{\frac{2}{3}} C_Z^{\delta_e} \cos \theta] \delta_e \\ [mx_G - (m + m_{33}) l_x] T_z + [(m + m_{33}) Q \nabla C_m^{\delta_e} - mx_G Q \nabla^{\frac{2}{3}} C_Z^{\delta_e} \cos \theta] \delta_e \end{bmatrix}}{[(m + m_{33})(I_y + m_{55}) - m^2 x_G^2]^2} \quad (11)$$

This is just a two-input-two-output system. Note that the virtual control vector has no direct effects on  $\theta$  and  $h$  because of (9), and then we can concentrate on the vector of  $z$ . The tracking of  $\theta$  and  $h$  can be achieved through a complete kinematic relationship when their references can be reformulated into the references of  $q$  and  $w$ , respectively, as illustrated in the following.

### 3.1.2. Aerodynamic Uncertainty Observer Design

Comparing with the relatively accurate aerodynamic actuator coefficients  $C_Z^{\delta_e}$  and  $C_m^{\delta_e}$ , the aerodynamic uncertainties in  $C_{m_0}$ ,  $C_m^\alpha$ ,  $C_m^q$ ,  $C_{Z_0}$  and  $C_Z^\alpha$  in  $h_1(x)$  and  $h_2(x)$  are quite large, especially for the low-speed stratospheric airships due to the rarefied gas effect within the stratosphere. In this scenario, the air flow has much more significant effects on these coefficients. In addition,  $\alpha$  is difficult to measure accurately and then to be used in the control law. Therefore, the control scheme should be rather insensitive to these aerodynamic uncertainties in the absence of  $\alpha$  measurement. In the popularly used feedback linearization, the straightforward thought is to eliminate  $h_1(x)$  and  $h_2(x)$  directly such that the plant (10) can be further reduced to two independent integrators, which can facilitate the subsequent controller design. Note that such an approach can also realize a dynamic decoupling for the effects of  $h_1(x)$  and  $h_2(x)$ . The extended state observer (ESO) proposed by Han [24,25] is an effective philosophy to deal with such problems without the accurate knowledge about these aerodynamic uncertainties. Consider

$$\begin{bmatrix} \dot{w} \\ \dot{q} \end{bmatrix} = \begin{bmatrix} h_1(x) \\ h_2(x) \end{bmatrix} + \begin{bmatrix} v_1 \\ v_2 \end{bmatrix} \quad (12)$$

and define  $z_1 = w$ ,  $z_2 = h_1(x)$ ,  $z_3 = q$ , and  $z_4 = h_2(x)$ , and then Equation (12) can be rewritten as

$$\begin{cases} \dot{z}_1 = z_2 + v_1 \\ \dot{z}_2 = \varepsilon_1 \\ \dot{z}_3 = z_4 + v_2 \\ \dot{z}_4 = \varepsilon_2 \end{cases} \quad (13)$$

Here,  $\varepsilon_1$  and  $\varepsilon_2$  are defined as two perturbations. Note that  $z_2$  and  $z_4$  can be regarded as extended states [24,25] without any explicit physical meanings. Therefore, it is unnecessary to model these two variables in their original forms. Instead, they can be viewed as signals rather than as mathematical models. In doing so, accurate information about the aerodynamics is not necessary any more. To eliminate  $z_2$  and  $z_4$ , we can design two linear observers for the  $w$  and  $q$  subsystems in (13) as [24,25]

$$\begin{cases} \begin{cases} \dot{\hat{z}}_1 = \hat{z}_2 + v_1 + 2\omega_w(z_1 - \hat{z}_1) + v_1 \\ \dot{\hat{z}}_2 = \omega_w^2(z_1 - \hat{z}_1) \end{cases} \\ \begin{cases} \dot{\hat{z}}_3 = \hat{z}_4 + v_2 + 2\omega_q(z_3 - \hat{z}_3) + v_2 \\ \dot{\hat{z}}_4 = \omega_q^2(z_3 - \hat{z}_3) \end{cases} \end{cases} \quad (14)$$

where  $\omega_w$  and  $\omega_q$  are the bandwidths of the two observers, respectively. The observer (14) is also called an extended state observer [24,25] because of the definition of the states of

$z_2$  and  $z_4$ . When the observers converge, we can assume that  $z_2 \approx \hat{z}_2$  and  $z_4 \approx \hat{z}_4$ . These estimations can be utilized in the subsequent controller design.

### 3.1.3. Decoupling Controller Design

We utilize the above observer estimation with the virtual control variables taking the following form of

$$\begin{cases} v_1 = v_1 - \hat{z}_2 \\ v_2 = v_2 - \hat{z}_4 \end{cases} \quad (15)$$

Equation (13) can be approximated as

$$\begin{cases} \dot{z}_1 \approx v_1 \\ \dot{z}_3 \approx v_2 \end{cases} \quad (16)$$

which are just two integrators, and the proportional controllers can be straightforwardly used as

$$\begin{cases} v_1 = k_w(w_r - w) \\ v_2 = k_q(q_r - q) \end{cases} \quad (17)$$

to achieve satisfactory tracking performance or zero steady-state with two proper positive gains of  $k_w$  and  $k_q$ , wherein  $w_r$  and  $q_r$  are their references, respectively. Combining (15) and (17) yields the virtual control law as

$$\begin{cases} v_1 = k_w(w_r - w) - \hat{z}_2 \\ v_2 = k_q(q_r - q) - \hat{z}_4 \end{cases} \quad (18)$$

In fact, the original control variables can be obtained through (11) as

$$\begin{bmatrix} T_z \\ \delta_e \end{bmatrix} = [(m + m_{33})(I_y + m_{55}) - m^2 x_G^2]^2 \begin{bmatrix} I_y + m_{55} - m x_G l_x & m x_G Q \nabla C_m^{\delta_e} - (I_y + m_{55}) Q \nabla^{\frac{2}{3}} C_Z^{\delta_e} \cos \theta \\ m x_G - (m + m_{33}) l_x & (m + m_{33}) Q \nabla C_m^{\delta_e} - m x_G Q \nabla^{\frac{2}{3}} C_Z^{\delta_e} \cos \theta \end{bmatrix}^{-1} \begin{bmatrix} k_w(w_r - w) - \hat{z}_2 \\ k_q(q_r - q) - \hat{z}_4 \end{bmatrix} \quad (19)$$

which is also a static decoupling process. This completes the coordinated control design, which provides a foundation for the following coordinated reference design.

### 3.2. Coordinated Reference Design

During the ascending phase, the altitude and the attitude should be simultaneously controlled. The control objectives of these two variables are different. The altitude has a specific reference to track, while the attitude should be stable without a specific reference. Therefore, the two objectives must be carefully coordinated to avoid conflict.

Considering the abovementioned control framework with regard to  $w$  and  $q$ , the altitude and the attitude references can be straightforwardly transformed into the references for  $w$  and  $q$  as

$$w_r = k_y(h_r - h) \quad (20)$$

$$q_r = k_\theta(\theta_r - \theta) \quad (21)$$

with two positive gains of  $k_y$  and  $k_\theta$ , where  $h_r$  and  $\theta_r$  are references for the altitude and the pitch, respectively. This is just the popularly used transformation from the position control to the speed control to speed up dynamic response. Thereafter, a new problem arises, how to coordinate  $w$  and the angular variable simultaneously or how to design the reference for  $\theta$ ? According to the heuristic knowledge from the symmetrical point of view, in fact, the pitch angle and the vertical speed are inherently consistent for a traditional flight vehicle. This consistency reflects that both curves have similar shapes, which is intrinsically embodied in the symmetrical kinematics of  $w = V \sin \gamma$  wherein  $\gamma$ (rad) is the elevation

angle. Because  $\gamma$  can be regarded as a lag output of the pitch, therefore, in nature,  $w \approx V\theta$  holds true and then we can design the  $\theta$  reference as

$$\theta_r = k_w w_r \quad (22)$$

with a scale factor  $k_w$ . This exhibits a natural coordination or a symmetry from the flight mechanics point of view, which should be fully utilized [29,30]. By doing so, the inconsistency between the altitude tracking and the attitude stability can be eliminated from the original source, and the kinematic symmetry plays a crucial role here.

#### 4. Stability Analysis

Here, the closed-loop performance is rigorously investigated in theory to provide an insightful viewpoint for the proposed design.

The following assumptions about the references  $w_r, q_r$  and disturbances  $h_1(x), h_2(x)$  are needed to conduct the stability analysis.

**Hypothesis 1.** There exists a known positive constant  $r_0$ , such that  $w_r, q_r$  satisfy

$$\|(w_r, q_r)\| \leq r_0$$

where  $\|\cdot\|$  represents the standard Euclidean norm.

**Hypothesis 2.** There exist the positive constants  $L_{10}, L_{11}, L_{20}, L_{21}$ , and the derivatives of total disturbances  $\dot{h}_1(x), \dot{h}_2(x)$  satisfy

$$|\dot{h}_1(x)| \leq L_{10}\|(w, q)\| + L_{11}, |\dot{h}_2(x)| \leq L_{20}\|(w, q)\| + L_{21}$$

**Theorem 1.** Under Assumption 1 and Assumption 2, the proposed design with ESO is bounded when  $1 - 2\lambda_{\max}(P)(L_{10} + L_{20}) > 0$  holds true, and the estimation error and the tracking error satisfy

$$\|E\| \leq \max \left\{ \frac{\sqrt{\lambda_{\max}(P)}}{\sqrt{\lambda_{\min}(P)}} \|E(t_0)\|, \frac{2\lambda_{\max}^2(P)[(L_{10} + L_{20})r_0 + (L_{11} + L_{21})]}{\lambda_{\min}(P)[1 - 2\lambda_{\max}(P)(L_{10} + L_{20})]} \right\}$$

where  $E$  includes both the estimation error and tracking error,  $\lambda_{\max}(P)$  and  $\lambda_{\min}(P)$  are the maximum and minimum eigenvalues of a positive definite matrix  $P$ . When  $t \rightarrow \infty$ , one has

$$\|E\| \leq \frac{2\lambda_{\max}^2(P)[(L_{10} + L_{20})r_0 + (L_{11} + L_{21})]}{\lambda_{\min}(P)[1 - 2\lambda_{\max}(P)(L_{10} + L_{20})]}$$

**Proof of Theorem 1.** Denote the tracking error

$$e_w = w_r - w \quad (23)$$

$$e_q = q_r - q \quad (24)$$

and the estimation error

$$\begin{cases} \tilde{z}_1 = z_1 - \hat{z}_1 \\ \tilde{z}_2 = z_2 - \hat{z}_2 = h_1(x) - \hat{z}_2 \end{cases} \quad (25)$$

$$\begin{cases} \tilde{z}_3 = z_3 - \hat{z}_3 \\ \tilde{z}_4 = z_4 - \hat{z}_4 = h_2(x) - \hat{z}_4 \end{cases} \quad (26)$$

Combining (18) and (23)–(26) has

$$\dot{e}_w = \dot{w}_r - \dot{w} = -k_w e_w - k_w \tilde{z}_1 - \tilde{z}_2 \quad (27)$$

$$\dot{e}_q = \dot{q}_r - \dot{q} = -k_q e_q - k_q \tilde{z}_3 - \tilde{z}_4 \quad (28)$$

And

$$\begin{aligned} \dot{\tilde{z}}_1 &= \dot{z}_1 - \dot{\hat{z}}_1 = \tilde{z}_2 - 2\omega_1 \tilde{z}_1 \\ \dot{\tilde{z}}_2 &= \varepsilon_1 - \omega_1^2 \tilde{z}_1 \end{aligned} \quad (29)$$

$$\begin{aligned} \dot{\tilde{z}}_3 &= \dot{z}_3 - \dot{\hat{z}}_3 = \tilde{z}_4 - 2\omega_2 \tilde{z}_3 \\ \dot{\tilde{z}}_4 &= \varepsilon_2 - \omega_2^2 \tilde{z}_3 \end{aligned} \quad (30)$$

Let  $E_w = [e_w \quad \tilde{z}_1 \quad \tilde{z}_2]^T$ ,  $E_q = [e_q \quad \tilde{z}_3 \quad \tilde{z}_4]^T$ , one obtains

$$\dot{E}_w = \begin{bmatrix} -k_w & -k_w & -1 \\ 0 & -2\omega_1 & 1 \\ 0 & -\omega_1^2 & 0 \end{bmatrix} E_w + \begin{bmatrix} 0 \\ 0 \\ 1 \end{bmatrix} \varepsilon_1 = A_w E_w + B_w \varepsilon_1 \quad (31)$$

and

$$\dot{E}_q = \begin{bmatrix} -k_q & -k_q & -1 \\ 0 & -2\omega_2 & 1 \\ 0 & -\omega_2^2 & 0 \end{bmatrix} E_q + \begin{bmatrix} 0 \\ 0 \\ 1 \end{bmatrix} \varepsilon_2 = A_q E_q + B_q \varepsilon_2 \quad (32)$$

Define  $E = [E_w^T \quad E_q^T]^T$ , then

$$\dot{E} = \begin{bmatrix} A_w & 0 \\ 0 & A_q \end{bmatrix} E + \begin{bmatrix} B_w \\ 0 \end{bmatrix} \varepsilon_1 + \begin{bmatrix} 0 \\ B_q \end{bmatrix} \varepsilon_2 = \Gamma E + B_1 \varepsilon_1 + B_2 \varepsilon_2 \quad (33)$$

Since  $\Gamma$  is Hurwitz, there exists a positive definite matrix  $P$  such that  $\Gamma^T P + P\Gamma = -I$ . According to Assumptions 1 and 2, the derivatives of  $h_1(x)$ ,  $h_2(x)$  satisfy

$$\begin{aligned} \varepsilon_1 &\leq L_{10}E + L_{10}r_0 + L_{11} \\ \varepsilon_2 &\leq L_{20}E + L_{20}r_0 + L_{21} \end{aligned}$$

Construct the Lyapunov function  $V = E^T P E$ , and taking its time derivative along the system (33) yields

$$\begin{aligned} \dot{V} &= \dot{E}^T P E + E^T P \dot{E} \\ &\leq -\|E\|^2 + 2\lambda_{\max}(P)\|E\|[(L_{10} + L_{20})\|E\| + (L_{10} + L_{20})r_0 + (L_{11} + L_{21})] \\ &\leq -[1 - 2\lambda_{\max}(P)(L_{10} + L_{20})]\|E\|^2 + 2\lambda_{\max}(P)[(L_{10} + L_{20})r_0 + (L_{11} + L_{21})]\|E\| \end{aligned} \quad (34)$$

Obviously,  $[1 - 2\lambda_{\max}(P)(L_{10} + L_{20})] > 0$  must be satisfied to guarantee the system stability. Considering  $\lambda_{\min}(P)\|E\|^2 \leq V \leq \lambda_{\max}(P)\|E\|^2$  has

$$\frac{\sqrt{V}}{\sqrt{\lambda_{\max}(P)}} \leq \|E\| \leq \frac{\sqrt{V}}{\sqrt{\lambda_{\min}(P)}} \quad (35)$$

Let  $W = \sqrt{V}$ , then  $\dot{W} = \frac{\dot{V}}{2\sqrt{V}}$ . Combining (34) and (35) can obtain

$$\dot{W} \leq -\frac{\sqrt{V}}{2\lambda_{\max}(P)} [1 - 2\lambda_{\max}(P)(L_{10} + L_{20})] + \frac{\lambda_{\max}(P)}{\sqrt{\lambda_{\min}(P)}} [(L_{10} + L_{20})r_0 + (L_{11} + L_{21})] \quad (36)$$

Due to  $W(t) = \int_{t_0}^t W(\tau) d\tau + W(t_0)$ , one has

$$\begin{aligned} \dot{W} &\leq -\frac{1 - 2\lambda_{\max}(P)(L_{10} + L_{20})}{2\lambda_{\max}(P)} \int_{t_0}^t \dot{W}(\tau) d\tau + \frac{\lambda_{\max}(P)}{\sqrt{\lambda_{\min}(P)}} [(L_{10} + L_{20})r_0 + (L_{11} + L_{21})] - \\ &\quad \frac{1 - 2\lambda_{\max}(P)(L_{10} + L_{20})}{2\lambda_{\max}(P)} W(t_0) \end{aligned} \quad (37)$$

Applying Gronwall–Bellman inequality [31] to (37) gives

$$\sqrt{V} \leq \int_{t_0}^t \frac{\lambda_{\max}(P)[(L_{10}+L_{20})r_0+(L_{11}+L_{21})]}{\sqrt{\lambda_{\min}(P)}} e^{-\frac{1-2\lambda_{\max}(P)(L_{10}+L_{20})}{2\lambda_{\max}(P)}(t-\tau)} d\tau + \sqrt{V(t_0)} e^{-\frac{1-2\lambda_{\max}(P)(L_{10}+L_{20})}{2\lambda_{\max}(P)}(t-t_0)} \quad (38)$$

which implies

$$\sqrt{V} \leq \frac{2\lambda_{\max}^2(P)[(L_{10}+L_{20})r_0+(L_{11}+L_{21})]}{\sqrt{\lambda_{\min}(P)}[1-2\lambda_{\max}(P)(L_{10}+L_{20})]} \left(1 - e^{-\frac{1-2\lambda_{\max}(P)(L_{10}+L_{20})}{2\lambda_{\max}(P)}(t-t_0)}\right) + \sqrt{V(t_0)} e^{-\frac{1-2\lambda_{\max}(P)(L_{10}+L_{20})}{2\lambda_{\max}(P)}(t-t_0)} \quad (39)$$

Since  $\|E\| \leq \frac{\sqrt{V}}{\sqrt{\lambda_{\min}(P)}}$ ,  $\sqrt{V(t_0)} \leq \sqrt{\lambda_{\max}(P)}\|E(t_0)\|$ , Equation (39) can be transformed into

$$\|E\| \leq \frac{2\lambda_{\max}^2(P)[(L_{10}+L_{20})r_0+(L_{11}+L_{21})]}{\lambda_{\min}(P)[1-2\lambda_{\max}(P)(L_{10}+L_{20})]} \left[1 - e^{-\frac{1-2\lambda_{\max}(P)(L_{10}+L_{20})}{2\lambda_{\max}(P)}(t-t_0)}\right] + \frac{\sqrt{\lambda_{\max}(P)}}{\sqrt{\lambda_{\min}(P)}} \|E(t_0)\| e^{-\frac{1-2\lambda_{\max}(P)(L_{10}+L_{20})}{2\lambda_{\max}(P)}(t-t_0)} \quad (40)$$

Then it can be concluded that

$$\|E\| \leq \max \left\{ \frac{\sqrt{\lambda_{\max}(P)}}{\sqrt{\lambda_{\min}(P)}} \|E(t_0)\|, \frac{2\lambda_{\max}^2(P)[(L_{10}+L_{20})r_0+(L_{11}+L_{21})]}{\lambda_{\min}(P)[1-2\lambda_{\max}(P)(L_{10}+L_{20})]} \right\} \quad (41)$$

when  $t \rightarrow \infty$ ,  $\lim_{t \rightarrow \infty} e^{-\frac{1-2\lambda_{\max}(P)(L_{10}+L_{20})}{2\lambda_{\max}(P)}(t-t_0)} = 0$ , thus

$$\|E\| \leq \frac{2\lambda_{\max}^2(P)[(L_{10}+L_{20})r_0+(L_{11}+L_{21})]}{\lambda_{\min}(P)[1-2\lambda_{\max}(P)(L_{10}+L_{20})]}$$

This completes the proof.  $\square$

## 5. Numerical Simulation

In this section, several simulations are carried out to validate the effectiveness of the proposed method.

The simulations were conducted on a Windows 11 based laptop, wherein the 11th Gen Intel(R) Core(TM) i7-1165G7 was used with the main frequency of 2.80 GHz and the RAM was 16G. The algorithms were encoded in Matlab 2021b environment. The Euler integral method was employed at the step size of 1 ms.

The initial altitude is 19,500 m, and the expected altitude is 20,000 m. Other initial states are as follows:  $\theta_i = 10^\circ$ ,  $u_i = 15$  m/s, and  $w_i = 18$  m/s. The characteristic parameters of the airship can be listed as [32]

$$\begin{aligned} m &= 5.6 \times 10^4 \text{ kg}, \quad \Xi = 7.4 \times 10^5 \text{ m}^3, \quad \rho = 0.089 \text{ kg/m}^3, \\ m_{33} &= 8.4 \times 10^4 \text{ kg}, \quad m_{55} = 8.4 \times 10^4 \text{ kg}, \quad I_y = 2.9 \times 10^8 \text{ kg} \cdot \text{m}^2, \\ C_{X_0} &= 0.0437, \quad C_{X^\alpha}^\alpha = 0.0 \text{ rad}^{-1} \\ C_{Z_0} &= 0.02, \quad C_{Z^\alpha}^\alpha = 1.269 \text{ rad}^{-1}, \quad C_{Z^{\delta_e}}^{\delta_e} = 0.2011 \text{ rad}^{-1} \\ C_{m_0} &= 0.0, \quad C_{m^\alpha}^\alpha = 0.2552 \text{ rad}^{-1}, \quad C_{m^q}^q = 0.2469 \text{ rad}^{-1} \cdot \text{s}, \quad C_{m^{\delta_e}}^{\delta_e} = -0.4310 \text{ rad}^{-1} \\ x_G &= 0 \text{ m}, \quad z_G = 5.0 \text{ m}, \quad l_x = 3.0 \text{ m} \end{aligned}$$

The actuator ranges are  $|\delta_e| \leq 20\text{deg}$  and  $|T_z| \leq 80\text{kN}$ .

At first, the guidance parameters are provided as  $k_y = 0.025$ ,  $k_w = 0.0097$  and  $k_\theta = 0.05$  to consider the time scale separation principle among different control loops such that inconsistency can be averted. It should be noted that a reference saturation of 20 m/s

is employed for  $w_r$  to ensure safety. As a result, the control parameters are also tuned as  $\omega_w = 2\text{rad/s}$ ,  $\omega_q = 5\text{rad/s}$ ,  $k_w = 0.2$ , and  $k_q = 0.6$ , respectively. For a similar reason, the saturations are also utilized for the control error terms of (17) to guarantee that the adverse scenario of a large control error and the intrinsic airship sluggish response cannot emerge and the potential harmful effects can be eliminated. Because the ESOs need time to converge, (17) is only used in the absence of the observers prior to 30 s; after 30 s, the two observers are switched in to enhance tracking accuracy.

#### (1) Effectiveness

The nominal case was analyzed based on the results shown in Figures 1–7. In Figure 1, it is observed that the altitude reaches 20 km at around 150 s, which indicates that the altitude tracking is successful. Figures 2 and 4 demonstrate that the vertical speed and the pitch angular rate can track their respective references satisfactorily, which implies that the control system is working effectively. Figure 3 reveals that the pitch regulation may seem sluggish, but it is important to note that the attitude stability is more critical than the specific attitude value in altitude tracking. The attitude controller mainly provides an attitude damping effect, which helps maintain the stability of the system.

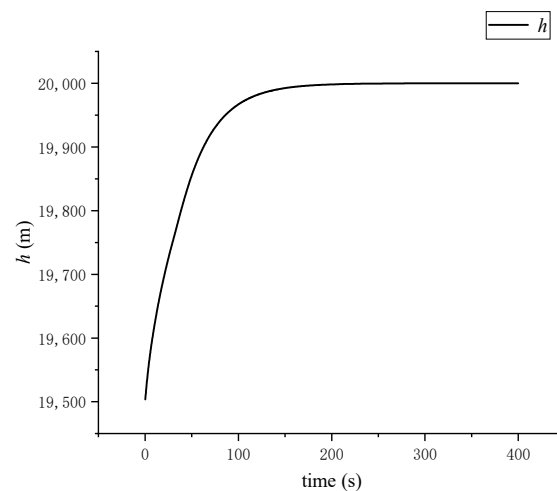


**Figure 1.** Altitude in the nominal case.

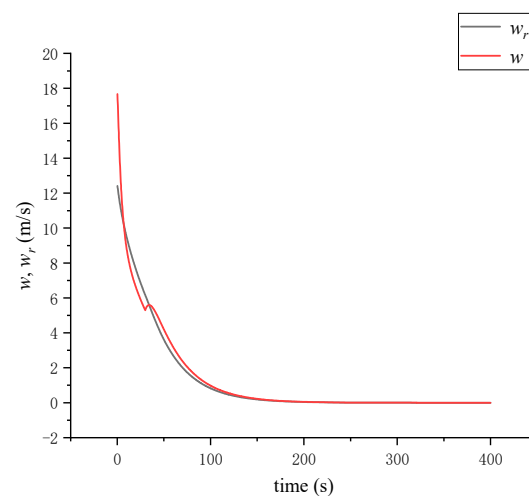


**Figure 2.** Vertical speed in the nominal case.

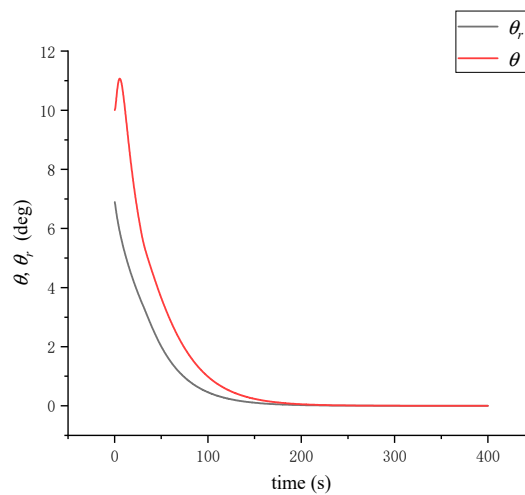


Figure 3. Pitch in the nominal case.

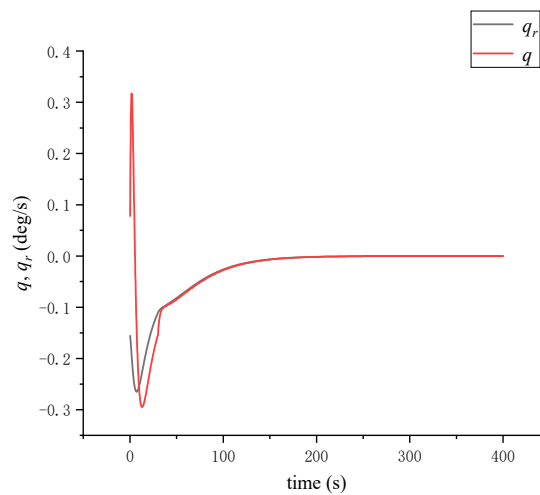


Figure 4. Pitch angular rate in the nominal case.

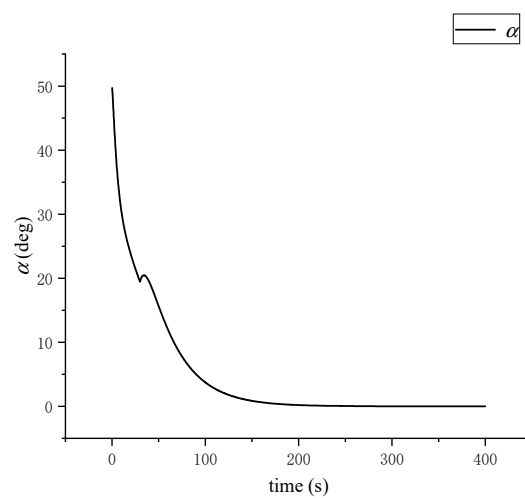


Figure 5. Angle of attack in the nominal case.

In Figures 6 and 7, it is observed that both actuators are operating within their reasonable ranges. This indicates that the control system is not overloading the actuators, which is a positive sign for the system's safety and longevity. Figure 8 shows that the vertical speed and the pitch have similar shapes, which suggests that they can be tightly matched when a

proper scale factor is used. This finding supports the key guidance reference coordination or an inherent symmetry between the altitude and the attitude in the paper. Overall, the results of the nominal case suggest that the control system is performing effectively and meeting the desired objectives.

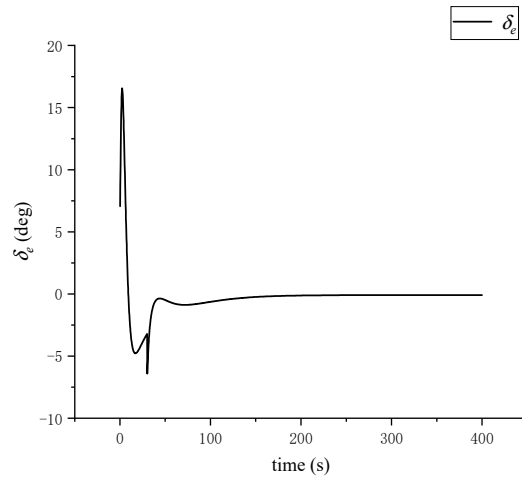


Figure 6. Elevator in the nominal case.

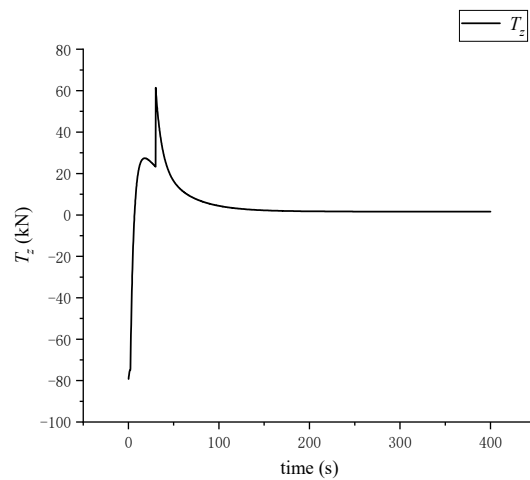


Figure 7. Vertical propeller thrust in the nominal case.

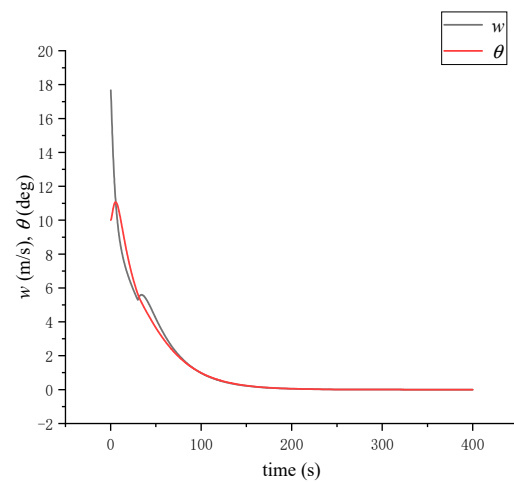


Figure 8. Vertical speed and pitch in the nominal case.

## (2) Comparison

To ensure a fair comparison, we decided to employ the controller without the ESO compensation throughout the entire flight. The results of this comparison are shown in Figure 9, which demonstrates that the altitude tracking performance is improved when the ESO compensation is switched in after 30 s. This suggests that the ESO compensation is effective in improving the altitude tracking performance.

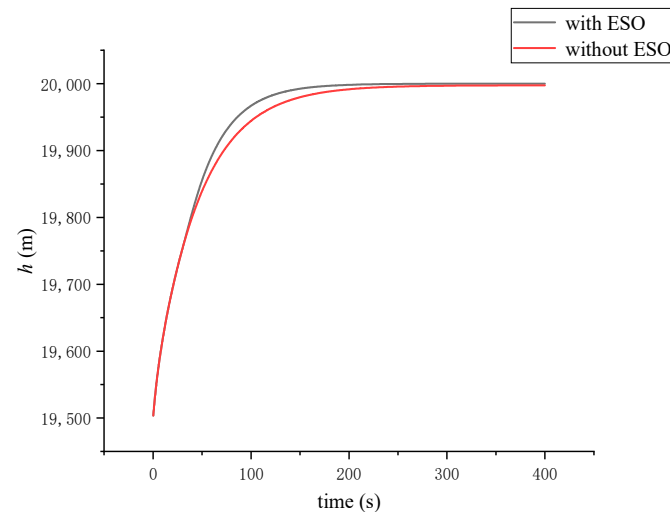


Figure 9. Two altitudes in comparison.

Furthermore, we also analyzed the performance of the vertical speed and the pitch angular rate controllers with and without ESO compensation. The results are shown in Figures 10 and 11. It can be observed that both controllers achieve better control performance when the ESO compensation is introduced. This finding suggests that the ESO compensation can significantly improve the control performance of the system.

In summary, the comparative analysis results indicate that the ESO compensation is effective in improving the altitude tracking performance, as well as the control performance of the vertical speed and pitch angular rate controllers. Therefore, the ESO compensation can be considered as an effective control strategy for enhancing the performance of the system.

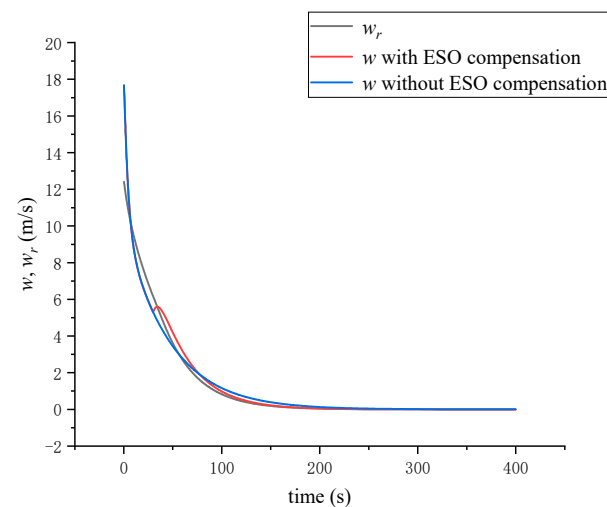
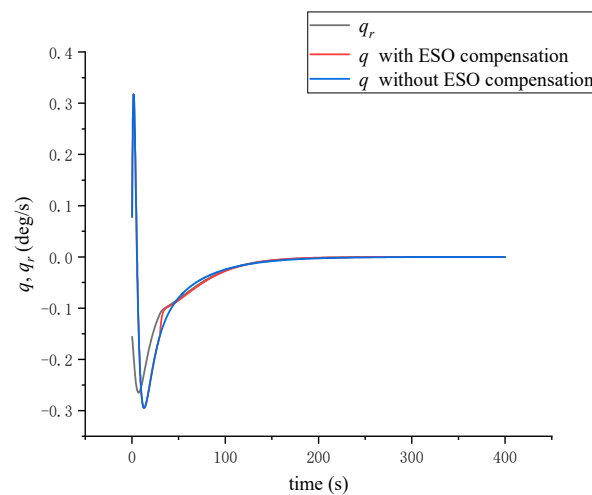


Figure 10. Two vertical speeds in comparison.



**Figure 11.** Two pitch angular rates in comparison.

### (3) Robustness

Finally, the aerodynamic uncertainties were considered to evaluate the robustness of the proposed method. In reality, there are two categories of aerodynamic uncertainties: one is the aerodynamic force, such as  $C_{Z_0}$  and  $C_Z^\alpha$ , and the other is the aerodynamic pitching moment of  $C_m$ . According to the empirical experience, the uncertainty ranges for various coefficients are usually rather diverse. The derivative coefficients of the aerodynamic force have much smaller uncertain ranges compared with those of  $C_m$ . In practice, 15% is the traditionally used uncertain range of the aerodynamic forces while 45% is of the aerodynamic moments. Note that  $C_m^q$  is the most inaccurate coefficient, and we set its uncertain range at  $-100\sim 200\%$ . Therefore, we evaluate the robustness of the system with perturbations shown in Table 1.

**Table 1.** Uncertain ranges in Monte Carlo simulation.

$C_{Z_0}$	$C_Z^\alpha$	$C_{m_0}$	$C_m^\alpha$	$C_m^q$
$\pm 15\%$	$\pm 15\%$	$\pm 45\%$	$\pm 45\%$	$-100\% \sim +200\%$

The Monte Carlo simulation results, as shown in Figures 12–16, demonstrate that the proposed guidance and control methods are capable of effectively dealing with diverse aerodynamic uncertainties, thereby achieving the objectives of the original design.

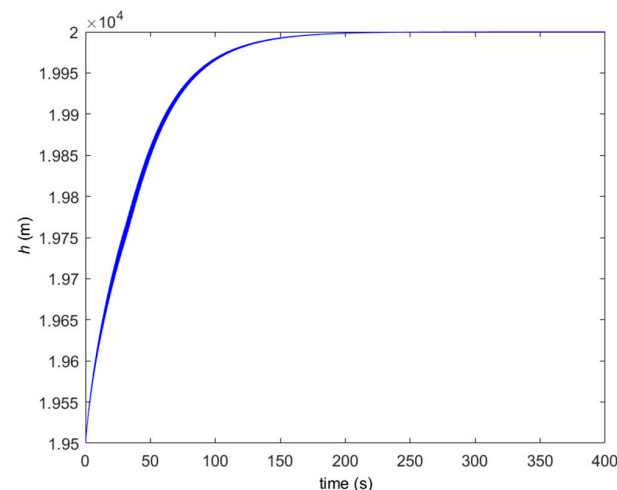


**Figure 12.** Altitudes in the Monte Carlo simulation.

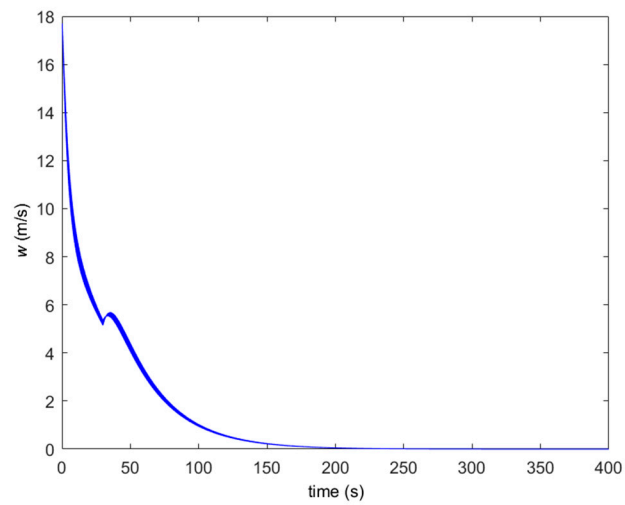


**Figure 13.** Vertical speeds in the Monte Carlo simulation.

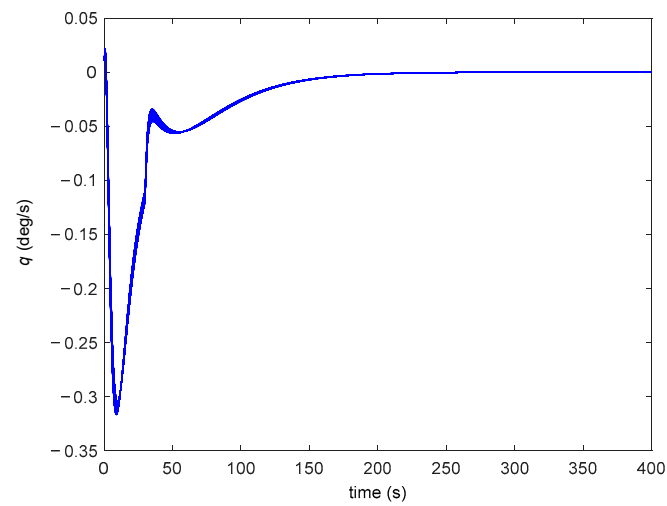


**Figure 14.** Pitch angular rates in the Monte Carlo simulation.

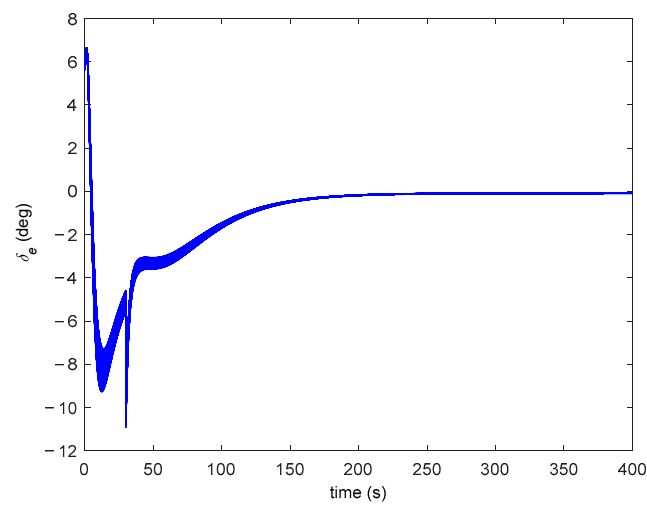


**Figure 15.** Elevators in the Monte Carlo simulation.

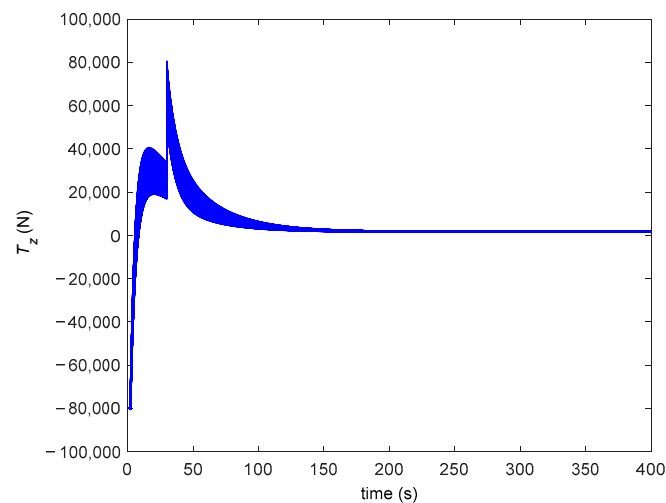


**Figure 16.** Propeller thrusts in the Monte Carlo simulation.

Figure 12 illustrates the altitude tracking performance of the proposed guidance and control methods under different levels of aerodynamic uncertainties. It can be observed that the altitude tracking error remains within the acceptable range, indicating the robustness of the proposed methods in dealing with aerodynamic uncertainties.

Figures 13 and 14 show the vertical speed and pitch angular rate tracking performance, respectively, under different levels of aerodynamic uncertainties. The results indicate that the proposed control methods can maintain good tracking performance for both variables, even under significant aerodynamic uncertainties.

Figures 15 and 16 demonstrate the elevators and the propeller thrusts, respectively, under different levels of aerodynamic uncertainties. It can be observed in Figure 15 that the elevator inputs remain within a reasonable range, which indicates that the control system is operating effectively, and the elevators are being utilized appropriately to maintain the desired performance. Figure 16 shows the propeller thrust inputs applied by the control system. It can be observed that the propeller thrust inputs remain within a reasonable range, implying that the control system is using the propeller thrust inputs appropriately to maintain the desired performance.

For a comparison, the Monte Carlo simulations under the same conditions without the ESO compensation were also conducted, and the results are illustrated from Figures 17–21, respectively. Comparing Figure 17 with Figure 12, it can be observed that the altitude covariance without the ESO compensation is obviously larger than that of the proposed method with slower responses. The integral-time-absolute-error (ITAE) index was utilized on the altitude, and the average ITAE indices are 19,356 and 22,887 for the proposed method and the one without the ESO compensation, respectively. Therefore, the ESO compensation effect is remarkable with an approximate 15% altitude ITAE cost reduction. Meanwhile, when comparing Figures 15 and 20 or comparing Figures 16 and 21, the actuators for the proposed method are a bit aggressive than the one in the absence of ESO compensation. This is a tradeoff because the proposed approach attempts to make full use of the actuators, and then the bandwidth of actuators should be addressed.

Overall, the Monte Carlo simulation results suggest that the proposed guidance and control methods are capable of effectively handling diverse aerodynamic uncertainties, ensuring the robustness and reliability of the system.

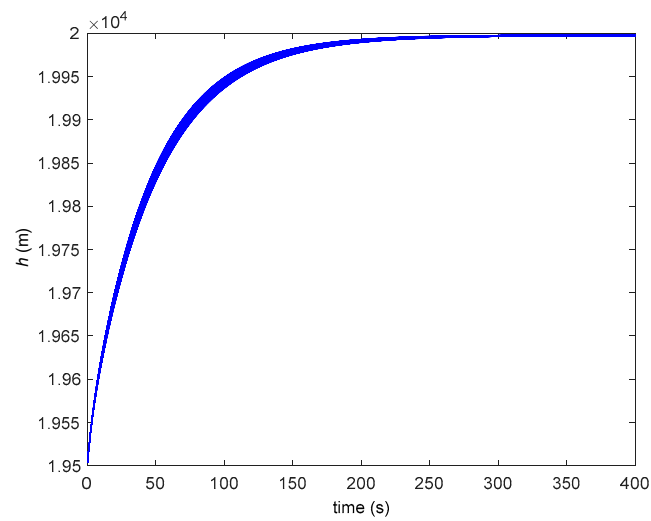


**Figure 17.** Altitudes in the Monte Carlo simulation without the ESO compensation.

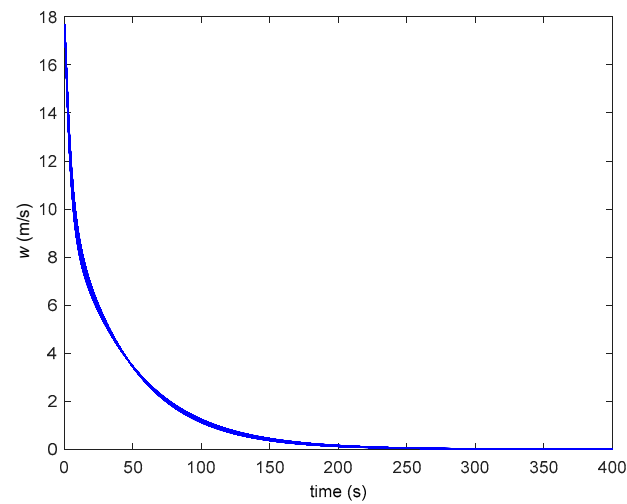


**Figure 18.** Vertical speeds in the Monte Carlo simulation without the ESO compensation.

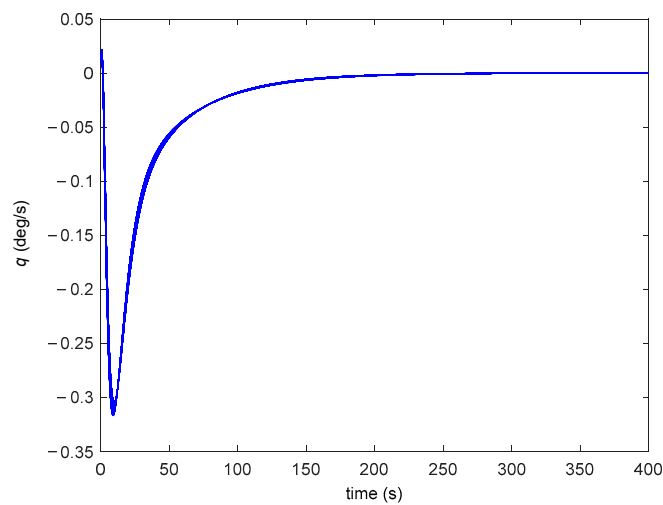


**Figure 19.** Pitch angular rates in the Monte Carlo simulation without the ESO compensation.

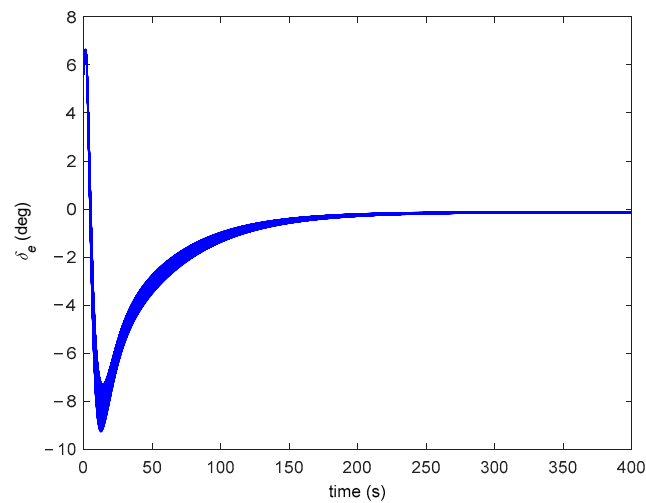


**Figure 20.** Elevators in the Monte Carlo simulation without the ESO compensation.

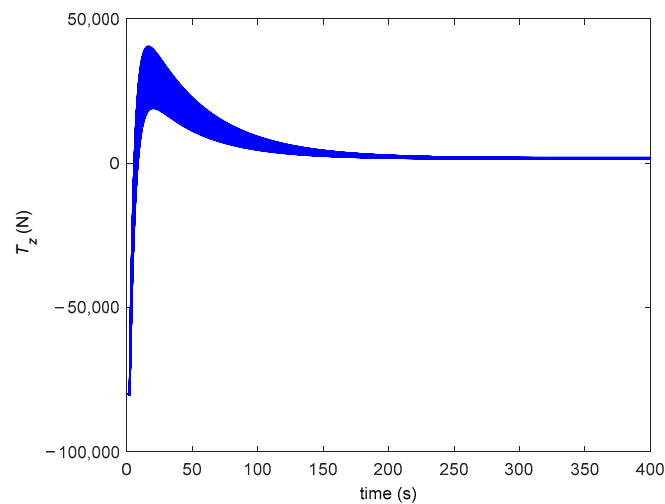


**Figure 21.** Propeller thrusts in the Monte Carlo simulation without the ESO compensation.

## 6. Conclusions

This paper presented a coordinated guidance and control method to realize the altitude position control for the stratospheric airship. The symmetrical characteristics of the airship were fully utilized to provide the inherently related references such that the altitude tracking, and the attitude stability could be simultaneously achieved. In this process, the direct control variables were the vertical speed and the pitch angular rate, which can speed up the response considerably to reduce the lag. To deal with the coupled control outputs, the static decoupling strategy was employed. The extended state observer was utilized to attenuate the strong aerodynamic uncertainties for the low-speed airship while the two actuators can yield symmetrical and concerted outputs. Rigorous theoretical investigation on the closed-loop performance was conducted to obtain explicit quantitative result. The extensive simulation results demonstrate the effectiveness of the proposed method, which can realize a 500-m altitude difference tracking within 200 s with less than 0.5 deg/s pitch angular rate. In the comparative simulations, an approximate 15% altitude ITAE cost reduction can be achieved, implying a better control performance. The proposed scheme could sufficiently utilize the actuator capability but at the cost of a high actuator bandwidth, which should be noted here. This practically comprehensive strategy might provide helpful guidelines for practitioners. This investigation is inspired by the inherent nature of airship symmetry.

In the future, the comprehensive energy efficient control strategy should be further sought and optimized. This is because both the elevator and the propeller thrust are driven by using onboard batteries, and as a result either reasonable energy distribution or optimal control coordination is crucial for the extended duration mission.

**Author Contributions:** Conceptualization, K.Y. and J.J.; methodology, K.Y., J.J. and M.S.; software, M.S.; validation, K.Y., M.S. and Z.C.; resources, K.Y.; writing—M.S. and Z.C.; visualization, M.S.; supervision, Z.C.; project administration, K.Y.; funding acquisition, M.S. All authors have read and agreed to the published version of the manuscript.

**Funding:** This research was funded by National Natural Science Foundation of China, grant number 62073177.

**Data Availability Statement:** The data presented in this study are available on request from the corresponding author.

**Conflicts of Interest:** The authors declare no conflict of interest.

## References

1. Politis, D.Z.; Potirakis, S.M.; Kundu, S.; Chowdhury, S.; Sasmal, S.; Hayakawa, M. Critical dynamics in stratospheric potential energy variations prior to significant ( $M > 6.7$ ) earthquakes. *Symmetry* **2022**, *14*, 1939. [\[CrossRef\]](#)
2. Griffin, D.K.; Swinyard, B.M.; Sidher, S.; Irwin, P. Feasibility study of a stratospheric-airship observatory. In Proceedings of the SPIE, Astronomical Telescopes and Instrumentation, Waikoloa, HI, USA, 3 March 2003.
3. Elfes, A.; Bueno, S.S.; Bergerman, M.; de Paiva, E.C.; Ramos, J.G.; Azinheria, J.R. Robotic airships for exploration of planetary bodies with an atmosphere: Autonomy challenges. *Auton. Robot.* **2003**, *14*, 147–164. [\[CrossRef\]](#)
4. Lv, M.; Li, J.; Zhu, W.; Du, H.; Meng, J.; Sun, K. A theoretical study of rotatable renewable energy system for stratospheric airship. *Energ. Convers. Manag.* **2017**, *140*, 51–61. [\[CrossRef\]](#)
5. Zhang, T.; Geng, S.; Mu, X.; Chen, J.; Wang, J.; Wu, Z. Thermal characteristics of a stratospheric airship with natural convection and external forced convection. *Int. J. Aerospace Eng.* **2019**, *2019*, 4368046. [\[CrossRef\]](#)
6. Shi, H.; Geng, S.; Qian, X. Thermodynamics analysis of a stratospheric airship with hovering capability. *Appl. Therm. Eng.* **2019**, *146*, 600–607. [\[CrossRef\]](#)
7. Mueller, J.B.; Paluszek, M.A. Development of an aerodynamic model and control law design for a high altitude airship. In Proceedings of the 3rd AIAA Unmanned Unlimited Technical Conference, Chicago, IL, USA, 20–23 September 2004.
8. De Paiva, E.; Benjovengo, F.; Bueno, S. Nonlinear control approaches for an autonomous unmanned robotic airship. In Proceedings of the 7th AIAA Aviation Technology, Integration and Operation Conference, Belfast, Northern Ireland, UK, 18–20 September 2007.
9. Kusagaya, T.; Fujii, H.; Kojima, H.; Watanabe, T.; Sakamoto, T. Nonlinear optimal control applied to longitudinal motion of an airship. In Proceedings of the 3rd AIAA Aviation Technology, Integration and Operation Conference, Denver, CO, USA, 17–19 November 2003.
10. Guo, J.; Zhou, J. Altitude control system of autonomous airships based on fuzzy logic. In Proceedings of the 2008 2nd International Symposium on Systems and Control in Aerospace and Astronautics, Shenzhen, China, 10–12 December 2008.
11. Fan, Y.; Yu, Y.; Yan, J. High altitude airship altitude control system design and simulation. *Appl. Mech. Mater.* **2011**, *128–129*, 142–145. [\[CrossRef\]](#)
12. Nie, C.; Zhu, M.; Zheng, Z.; Wu, Z. Model-free altitude control for airship based on Q-learning and CAMC network. In Proceedings of the 2016 IEEE Chinese Guidance, Navigation and Control Conference, Nanjing, China, 12–14 August 2016.
13. Schmidt, D. Modeling and near-space stationkeeping control of a large high-altitude airship. *J. Guid. Control Dynam.* **2007**, *30*, 540–547. [\[CrossRef\]](#)
14. Suleimenov, K.; Do, T.D. A practical disturbance rejection control scheme for permanent magnet synchronous motors. *Symmetry* **2022**, *14*, 1873. [\[CrossRef\]](#)
15. Tusset, A.M.; Inacio, D.; Fuziki, M.E.K.; Costa, P.M.L.Z.; Lenzi, G.G. Dynamic analysis and control for a bioreactor in fractional Order. *Symmetry* **2022**, *14*, 1609. [\[CrossRef\]](#)
16. Zhang, Y.; Qu, W.; Xi, Y.; Cai, Z. Adaptive stabilization and trajectory tracking of airship with neutral buoyancy. *Acta Autom. Sin.* **2008**, *34*, 1437–1441. [\[CrossRef\]](#)
17. Aguiar, A.P.; Hespanha, J.P. Trajectory-tracking and path-following of underactuated autonomous vehicles with parametric modeling uncertainty. *IEEE T. Automat. Contr.* **2007**, *52*, 1362–1379. [\[CrossRef\]](#)
18. Moutinho, A.; Azinheira, J.R.; de Paiva, E.C.; Bueno, S.S. Airship robust path-tracking: A tutorial on airship modelling and gain-scheduling control design. *Control Eng. Pract.* **2016**, *50*, 22–36. [\[CrossRef\]](#)
19. Zheng, Z.; Huo, W. Planar path following control for stratospheric airship. *IET Control Theory Appl.* **2013**, *7*, 185–201. [\[CrossRef\]](#)
20. Chen, T.; Zhu, M.; Zheng, Z. Asymmetric error-constrained path-following control of a stratospheric airship with disturbances and actuator saturation. *Mech. Syst. Signal Pr.* **2019**, *119*, 501–522. [\[CrossRef\]](#)

21. Zhu, E.; Pang, J.; Sun, N.; Gao, H.; Sun, Q.; Chen, Z. Airship horizontal trajectory tracking control based on active disturbance rejection control (ADRC). *Nonlinear Dynam.* **2014**, *75*, 725–734. [[CrossRef](#)]
22. Yang, Y. A time-specified nonsingular terminal sliding mode control approach for trajectory tracking of robotic airships. *Nonlinear Dynam.* **2018**, *92*, 1359–1367. [[CrossRef](#)]
23. Nie, C.; Zheng, Z.; Zhu, M. Three-dimensional path-following control of a robotic airship with reinforcement learning. *Int. J. Aerospace Eng.* **2019**, *2019*, 7854173. [[CrossRef](#)]
24. Han, J. From PID to active disturbance rejection control. *IEEE Trans. Ind. Electron.* **2009**, *56*, 900–906. [[CrossRef](#)]
25. Gao, Z. Scaling and bandwidth-parameterization based controller tuning. In Proceedings of the American Control Conference, Denver, CO, USA, 4–6 June 2003.
26. Li, Y.; Nahon, M.; Sharf, I. Airship dynamics modeling: A literature review. *Prog. Aerosp. Sci.* **2011**, *47*, 217–239. [[CrossRef](#)]
27. Gomes, S.B. An Investigation of the Flight Dynamics of Airship with Application to the YEZ-2A. Doctoral Thesis, Cranfield University, Cranfield, UK, 1990.
28. Li, Y.; Nahon, M.; Sharf, I. Dynamics modeling and simulation of flexible airship. *AIAA J.* **2009**, *47*, 592–605. [[CrossRef](#)]
29. Sun, M.; Zhang, Y.; Liu, J.; Huang, J.; Wang, Z.; Chen, Z. Explicit parameterized energy management for scramjet transition. *IEEE T. Aero. Elec. Sys.* **2019**, *55*, 798–809. [[CrossRef](#)]
30. Gong, Z.; Wang, Z.; Yang, C.; Li, Z.; Dai, M.; Zhang, C. Performance analysis on the small-scale reusable launch vehicle. *Symmetry* **2022**, *14*, 1862. [[CrossRef](#)]
31. Khalil, H. *Nonlinear Systems*, 3rd ed.; Prentice Hall: Hoboken, NJ, USA, 2002; pp. 651–652.
32. Ouyang, J. Research on Modeling and Control of an Unmanned Airship. Ph.D. Thesis, Shanghai Jiaotong University, Shanghai, China, 2003.

**Disclaimer/Publisher’s Note:** The statements, opinions and data contained in all publications are solely those of the individual author(s) and contributor(s) and not of MDPI and/or the editor(s). MDPI and/or the editor(s) disclaim responsibility for any injury to people or property resulting from any ideas, methods, instructions or products referred to in the content.